Nghiên cứu phân tán vật liệu SiO_2/g-C_3N_4 trên nền polyvinylidene fluoride và hoạt tính quang xúc tác phân hủy dung dịch RhB trong môi trường nước

TÓM TẮT

Vật liệu SiO_2/g-C_3N_4 được phân tán lên màng polyvinylidene fluoride (PVDF) bằng phương pháp đảo pha thu được màng quang xúc tác phân hủy chất màu hữu cơ rhodamnie B (RhB) trong môi trường nước dưới vùng ánh sáng khả kiến. Hình thái, cấu trúc và hoạt tính quang xúc tác của các vật liệu đơn và composite phân tán lên màng PVDF được đánh giá. Với vật liệu composite SiO_2/g-C_3N_4 có tính chất xốp hơn, có nhiều vị trí khuyết tật hơn so với các vật liệu SiO_2 hay g-C_3N_4 đơn chất khi phân tán lên màng làm cải thiện đáng kể hiệu quả quang xúc tác của vật liệu. Cụ thể, hiệu suất phân hủy RhB khỏi màng composite SiO_2/g-C_3N_4/PVDF dưới tác động của ánh sáng khả kiến đạt 81,35% vượt trội hơn so với g-C_3N_4/PVDF (46,07%) và SiO_2/PVDF (14,79%). Do đó, nghiên cứu này được kỳ vọng sẽ mở rộng triển vọng trong lĩnh vực công nghệ lọc màng.

Từ khóa: *SiO_2, g-C_3N_4, SiO_2/g-C_3N_4, PVDF*

Study on dispersion of SiO_2/g-C_3N_4 on polyvinylidene fluoride substrate and photocatalytic activity in decomposing RhB solution in aqueous environment

ABSTRACT

SiO_2/g-C_3N_4 material was dispersed onto polyvinylidene fluoride (PVDF) membrane by the phase inversion method to obtain a photocatalytic membrane for decomposing organic dye rhodamine B (RhB) in aqueous medium under visible light. The morphology, structure, and photocatalytic activity of single and composite materials deposited on PVDF membranes were evaluated. With SiO_2/g-C_3N_4 composite material having more porous properties and more defect locations than single SiO_2 or g-C_3N_4 materials when dispersed onto the membrane, the photocatalytic efficiency of the material is significantly improved. Specifically, the degradation efficiency of RhB from SiO_2/g-C_3N_4/PVDF composite membrane under the influence of visible light reached 81.35%, which was superior to g-C_3N_4/PVDF (46.07%) and SiO_2/PVDF (14.79%). Therefore, this study is expected to expand the prospects in the field of membrane filtration technology.

Keywords: *SiO_2, g-C_3N_4, SiO_2/g-C_3N_4, PVDF*

1. INTRODUCTION

Water pollution by persistent organic compounds – dyes, pesticides, and pharmaceutical residues – is becoming one of the most serious environmental challenges today. These compounds are often highly toxic, difficult to biodegrade, and accumulate in the environment for long, requiring effective and eco-friendly treatment methods.[1] Among modern treatment technologies, heterogeneous photocatalysis under visible light is a promising method due to its ability to completely decompose organic pollutants into non-toxic products such as CO_2 and H_2O without leaving secondary residues.[2, 3] In the field of photocatalytic materials, graphitic carbon nitride (g-C_3N_4) is considered a potential candidate due to its narrow band gap (~2.7 eV), good visible light absorption, high chemical stability, and simple synthesis from precursors such as melamine or urea.[4] However, g-C_3N_4 has limitations, typically low surface area, poor adsorption capacity, and a fast recombination rate of electron pairs.[5] To improve the catalytic efficiency, forming composite materials between g-C_3N_4 and supporting materials is considered an effective strategy. Silicon dioxide (SiO_2) – a potential semi-doped material with a porous structure, large surface area, and high stability – not only enhances the dispersion of g-C_3N_4 but also improves the charge transfer process in the photocatalytic reaction.[6, 7] Similar to SiO_2, several approaches have been taken to improve the photocatalytic activity of g-C_3N_4, including incorporating dopants and coupling with other semiconductors. Extensive efforts have been devoted to improving the photocatalytic activity of g-C_3N_4, and numerous novel g-C_3N_4-based photocatalysts have been reported, such as ZnO/g-C_3N_4 [8], $SmVO_4$/g-C_3N_4 and TaON/g-C_3N_4.[9-11] These photocatalysts were mainly developed based on the coupling effect. In addition, metal or non-metal element doping is typically used to improve the photoactivity of g-C_3N_4 (such as g-C_3N_4 and Fe–g-C_3N_4), [12, 13], which is based on energy band engineering. The hybridization of SiO_2 and g-C_3N_4 achieves a synergistic effect to overcome the major disadvantages of each material and create composite materials with good photocatalytic activity. In treating polluted water, the direct use of catalysts has the advantage of very high photocatalytic activity. However, these materials are still in powder form. Hence, they are challenging to recycle after the photocatalytic process.[14, 15] This causes significant waste of photocatalysts but also causes secondary pollution to the environment. Therefore, finding solutions to the problem of material recovery is of interest to researchers. Several methods for recovering inorganic photocatalysts have been reported, such as adding magnetic materials, forming rigid, recyclable, and flexible thin film materials, and loading them onto organic polymer materials [16, 17]. The major drawback of immobilizing the catalyst materials onto the substrate is the reduction of the active site, and the durability of the catalyst materials with the substrate is also of great concern. Poly(vinylidene fluoride) (PVDF) is a fluoropolymer with good chemical stability, good mechanical properties, and easy to process into films, which is very suitable as a substrate for membrane-based photocatalyst systems, which helps to improve the applicability and reusability [18]. In this study, $SiO_2/g\text{-}C_3N_4$ composite materials loaded onto PVDF were synthesized by a simple phase inversion method. This study focused on the synthesis, chemical characterization, and evaluation of the treatment performance of $SiO_2/g\text{-}C_3N_4$/PVDF materials for typical organic compounds in wastewater such as RhB, enhancing the photocatalytic activity under visible light, and improving the stability and recovery of materials after treatment.

2. EXPERIMENTAL

2.1. Material synthesis

Chemicals: All chemicals used for material synthesis include urea ($(NH_2)_2CO$), TEOS (Tetraethyl orthosilicate) ($C_8H_{20}O_4Si$), CTAB (Hexadecyl trimethyl ammonium bromide), ($[(C_{16}H_{33})N(CH_3)_3]Br$), polyvinylidene fluoride (PVDF), N-Methy-2-pyrrolidone (NMP) and rhodamine B ($C_{28}H_{31}ClN_2O_3$), Merck.

2.2. Materials synthesis:

2.2.1. Synthesis of g-C_3N_4 material

g-C_3N_4 material was prepared by a simple method using urea as raw material. The first, 10 grams of finely ground urea then transferred into alumina crucible, sealed with aluminum foil and calcined at 550 ºC for 1 hour. The solid obtained was pale yellow, washed with distilled water and ethanol, then dried at 80 ºC for 12 hours. The product is finely ground and marked g-C_3N_4.

2.2.2. Synthesis of SiO_2 material

SiO_2 material is synthesized according to the following process: Add 0.16 g of hexadecyl trimethyl ammonium bromide (CTAB) to 50 mL of distilled water, then slowly add 15 mL of ethanol and 1 mL of solution. Stir for 0.5 hour, slowly add 1 mL tetraethyl orthosilicate (TEOS) dropwise into the solution, and stir for 24 hours. The obtained product was washed with deionized water and ethanol three times, dried for 24 h at 60 ºC, and denoted SiO_2.

2.2.3. *Synthesis of* $SiO_2/g\text{-}C_3N_4$ *composite material*

Samples were prepared by a simple method using SiO_2 powder and urea as precursors. First, a mixture of 0.1g SiO_2 and 3g urea into an agate mortar and grind finely. Then, the as-prepared mixtures were then transferred into an alumina crucible, sealed with aluminum foil, and heat it in an inert Ar gas environment at 550 ºC for 1 hour. Cool to room temperature, grind and wash the sample with distilled water until neutral. The solid was dried at 80 ºC for 12 hours and denoted as $SiO_2/g\text{-}C_3N_4$.

2.2.4. Synthesis of $SiO_2/g\text{-}C_3N_4$/PVDF material

$SiO_2/g\text{-}C_3N_4$/PVDF material was prepared using the following procedure. Firstly, put 0.1g of $SiO_2/g\text{-}C_3N_4$ material into a glass jar with a lid, add 5 mL of NMP solution, and sonicate for 10 minutes. Then stir well on a magnetic stirrer for 30 minutes. Continue ultrasonic vibration for another 20 minutes and stir evenly on a magnetic stirrer for 20 minutes. Continue ultrasonic vibration for another 20 minutes and stir evenly on a magnetic stirrer for 20 minutes. Then let the mixture sit for 3 hours. Using a stainless steel scraper (250 µm x 15 cm), roll the mixture evenly onto the glass to form a composite film, quickly put the glass with the film into water to perform the phase reversal process, and the material is denoted as $SiO_2/g\text{-}C_3N_4$/PVDF.

2.3. Material characterization

The synthesized materials were characterized using several techniques. Infrared spectroscopy IR was performed on a Shimadzu IR Prestige-21. The crystal phase was analyzed by X-ray diffraction (XRD) using a Siemens D-500 Bruker system. Scanning electron microscopy (SEM) and X-ray energy dispersive spectroscopy (EDS) were conducted using a JSM-7600F device. Photoluminescence (PL) spectra were measured on a Hitachi F-7000 instrument with an excitation wavelength of 360 nm.

2.4. Photocatalytic evaluation

The photocatalytic activity of the obtained materials was evaluated by the decomposition of Rhodamine B (RhB) in an aqueous solution under visible light irradiation. Materials containing 0.1 g of the photocatalyst were added to 100 mL of RhB solution with a concentration of 10 mg/L and stirred in the dark for 60 minutes to achieve adsorption-desorption equilibrium. The photocatalytic process was then initiated under a 40W LED light. Every 30 minutes, 7 mL of the solution was centrifuged to remove the solid part. The concentration of RhB in the solution was determined on a UV-Vis meter (CE-2011) at a wavelength of 553 nm.

3. RESULTS AND DISCUSSION

3.1. Material characteristics

The crystal structures and phase compositions of the synthesized SiO_2, $g\text{-}C_3N_4$, $SiO_2/g\text{-}C_3N_4$ powders, and PVDF, SiO_2/PVDF, $g\text{-}C_3N_4$/PVDF, and $SiO_2/g\text{-}C_3N_4$/PVDF films are shown in Figure 1.

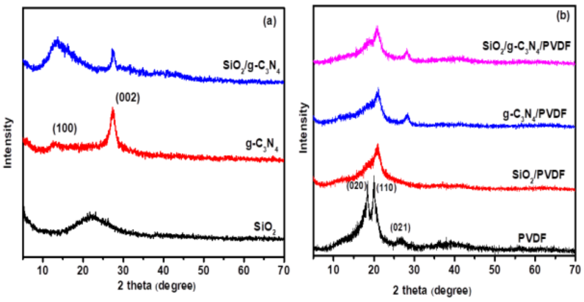

Figure. 1. (a) XRD patterns of SiO_2, $g\text{-}C_3N_4$, $SiO_2/g\text{-}C_3N_4$ and (b) PVDF, SiO_2/PVDF, $g\text{-}C_3N_4$/PVDF and $SiO_2/g\text{-}C_3N_4$/PVDF.

Figure 1a shows that the SiO_2 material exhibits a broad peak at $2\theta \approx 23°$ corresponding to the amorphous nature of SiO_2.[19] $g\text{-}C_3N_4$ shows typical diffraction peaks corresponding to the (002) and (100) planes of $g\text{-}C_3N_4$.[20] Specifically, the peak at $2\theta = 13.5°$ can be attributed to the in-plane structural stacking motif in the tri-s-triazine (s-heptazine)-based structure of $g\text{-}C_3N_4$, while the strong diffraction peak located at $2\theta = 27.6°$ is a result of the inter-plane stacking of the conjugated aromatic units of $g\text{-}C_3N_4$.[21] XRD results of $SiO_2/g\text{-}C_3N_4$ composite material fully show the characteristic peaks of both $g\text{-}C_3N_4$ and SiO_2. The SiO_2 peak at 23° is not clearly shown in the composite sample, possibly due to the amorphous SiO_2 structure and the stacking of $g\text{-}C_3N_4$. Thus, the SiO_2 added to the $g\text{-}C_3N_4$ substrate does not change the crystal structure. The results in Figure 1b show that PVDF has 3 characteristic peaks at 18.5°, 20.1°, 26.7° corresponding to the planes (020), (110), (021). When dispersing $g\text{-}C_3N_4$, SiO_2, $SiO_2/g\text{-}C_3N_4$ onto PVDF polymer matrix, the PVDF peaks still appear at almost the same position but the intensity is reduced. For the $g\text{-}C_3N_4$/PVDF sample, a characteristic strong peak at 27.6° and a weak peak at 13.5° corresponding to the (002) and (100) reflection planes of graphite-structured materials appear.[22]

Figure 2 shows the FT-IR spectrum of the synthesized material samples, demonstrating no change in the PVDF polymer structure.

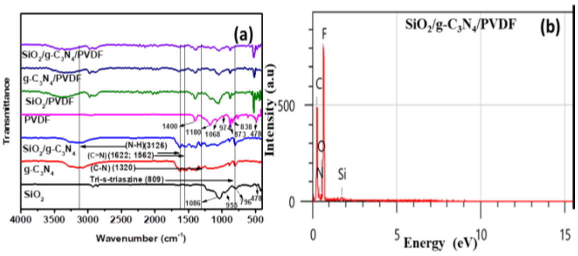

Figure 2. (a) FT–IR spectra of SiO_2, $g\text{-}C_3N_4$, $SiO_2/g\text{-}C_3N_4$, PVDF, SiO_2/PVDF, $g\text{-}C_3N_4$/PVDF, $SiO_2/g\text{-}C_3N_4$/PVDF, and (b) EDX spectra of $SiO_2/g\text{-}C_3N_4$/PVDF.

The FT-IR spectrum of pure PVDF shows the combination of α and β phases. The characteristic absorption bands for the α form are 1180 and 974 cm^{-1}, and for the β form are 1400, 1068, 873, and 838 cm^{-1}. The absorption bands at 1400, 873 cm^{-1} represent the valence vibration of the C-F bond, at 1180 and 487 cm^{-1} represent the C-C bond and the bending vibration of CF_2. These absorption bands are present in all FT-IR spectra of the material films without any structural changes, which may be caused by chemical bonding. Furthermore, the FT-IR spectra of SiO_2/PVDF and $g\text{-}C_3N_4$/PVDF materials showed characteristic absorption bands for $g\text{-}C_3N_4$ and SiO_2. Typical absorption bands for $g\text{-}C_3N_4$ are located at 3126 cm^{-1} corresponding to N–H groups, at 1622 and 1562 cm^{-1} belonging to C=N bonds, at 1320 cm^{-1} corresponding to C–H bonds, and the absorption band at 809 cm^{-1} corresponding to tri-s-triazine units. [23]

In the IR spectrum of SiO_2, strong absorption bands appear at wave numbers 1086, 955, and 796 cm^{-1} corresponding to the bonds of Si-O-Si, the deformation vibration of Si-OH, and the symmetric valence vibration of the Si-O bond. The peak observed at 478 cm^{-1} in the composite film material is related to the Si–O–Si stretching vibration of SiO_2. [24]

SEM images show a clear difference in the distribution of materials on the polymer membrane. PVDF material (Figure 3a) has a reasonably smooth surface with a uniform surface structure and is applied as a good substrate membrane. Figure 3b shows that the SiO2 particles are relatively uniformly distributed in the PVDF matrix. The surface of the material becomes more porous and increases the surface area. The g-C_3N_4 material is in sheet form, so when dispersed on the PVDF substrate (Figure 3c), it creates density heterogeneity, large particle clusters, uneven structure, and increases the material's porosity. The combination of SiO_2 and g-C_3N_4 (Figure 3d) shows a significantly more porous surface, showing dispersed phases and many defect sites. This improves the photocatalytic properties, mechanical strength, and membrane permeability.

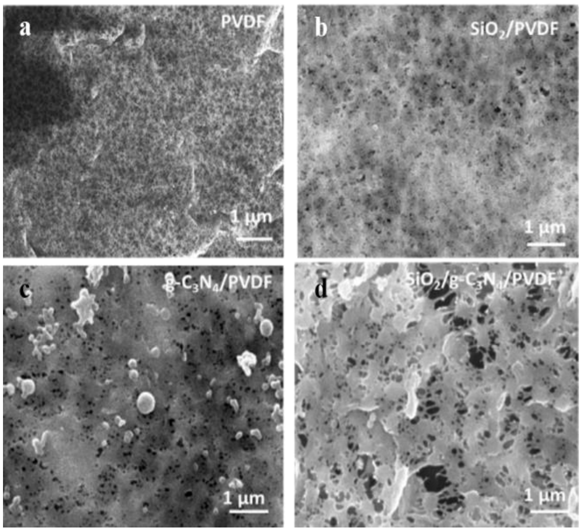

Figure 3. SEM images of PVDF (a), SiO_2/PVDF (b), g-C_3N_4/PVDF (c), SiO_2/g-C_3N_4/PVDF (d).

Energy dispersive X-ray (EDX) spectrum was characterized for the SiO_2/g-C_3N_4/PVDF composite sample (Figure 2b). The results from EDX images show the full presence of elements F, C, O, Si, and N in the sample, proving the successful synthesis of the material.

PL spectra of the materials were performed with an excitation wavelength of 390 nm at room temperature to study the photogenerated electron-hole recombination, and solid UV-Vis spectra determined the band gap energy of the materials, as shown in Figure 4.

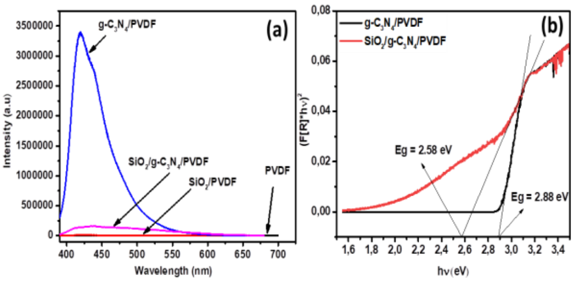

Figure. 4. (a) PL spectra of g-C_3N_4/PVDF, SiO_2/PVDF, PVDF, SiO_2/g-C_3N_4/PVDF (a) and (b) Band gap energy of g-C_3N_4/PVDF, SiO_2/g-C_3N_4/PVDF.

For PVDF, no PL intensity was observed over the entire spectral range. The g-C_3N_4 particles dispersed on the PVDF membrane have a maximum intensity corresponding to a wavelength of 419 nm, where the molecules with amino groups, such as g-C_3N_4, the nucleophile attack of the amino group on the carbon atom will lead to the nucleophile substitution of fluorine to form a covalent bond between PVDF and g-C_3N_4. The observed PL intensity of g-C_3N_4 is higher, which indicates a faster recombination rate between photogenerated electrons and holes. As for the PL spectrum of SiO_2/PVDF, the emission intensity is very low, almost equivalent to the PL spectrum of PVDF. This is explained by the fact that SiO_2 has a significant band gap energy and poor photocatalytic activity in the visible light region. On the other hand, the PL spectrum of the SiO_2/g-C_3N_4/PVDF composite material has a reduced fluorescence emission intensity compared to g-C_3N_4/PVDF (Figure 4a) and the band gap energy of the SiO_2/g-C_3N_4/PVDF material (Eg = 2.58 eV) is lower than that of g-C_3N_4/PVDF (Eg = 2.88 eV) (Figure 4b). Therefore, when there is radiation, electrons move from g-C_3N_4 to the conduction band of SiO_2 and then quickly move to the catalyst's surface to perform a reduction reaction with oxygen molecules, limiting the ability to recombine.

3.2. Photocatalytic performance

The results of the photocatalytic evaluation for PVDF, g-C_3N_4/PVDF, and C/g-C_3N_4/PVDF are shown in Figure 5.

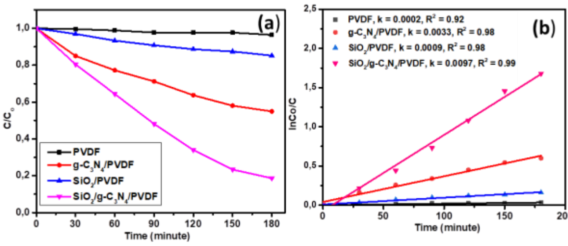

Figure 5. (a) RhB decomposition and (b) pseudo-first-order kinetic model under visible light of g-PVDF, C_3N_4/PVDF, SiO_2/g-C_3N_4, and SiO_2/g-C_3N_4/PVDF.

The graph shows that after 180 minutes of illumination under a 40W LED lamp, the decomposition efficiency of RhB solution of SiO_2/g-C_3N_4/PVDF sample is the highest at 81.35%, the materials g-C_3N_4/PVDF, SiO_2/PVDF have decomposition efficiency of 46.07% and 14.79% respectively. This may be because the band gap energy of the SiO_2/g-C_3N_4/PVDF material (2.58 eV) is lower than the band gap energy of the g-C_3N_4 material (2.88 eV), which makes the ability to separate and move photogenerated electrons and holes to the material surface to perform reactions faster, limiting the ability to recombine between charge carriers. SiO_2/PVDF material works well in the ultraviolet region, which is understandable because the photocatalytic efficiency in the visible light region is only 14.79%. The PVDF membrane alone did not show photocatalytic activity, indicating that the photocatalytic activity was due to the composite material; the single dispersed materials were exhibited. The kinetic model of RhB degradation of SiO_2/g-C_3N_4/PVDF material has a rate constant of 0.0097 (min^{-1}) which is much larger than that of C_3N_4/PVDF and SiO_2/PVDF materials (0.0033 and 0.0009 min^{-1}) (Figure 5b). A comparison of the rate constant of the present work with the previous works is listed in Table S1. However, the comparison is lame because the reaction conditions are not the same. However, Table S1 shows that the rate constant of SiO_2/g-C_3N_4/PVDF is relatively high compared to previous studies. This result confirms the potential application of SiO_2/g-C_3N_4/PVDF material in the treatment of organic pollutants under visible light in aquatic environments.

4. CONCLUSION

In this study, PVDF composite films modified with SiO_2 and g-C_3N_4 were successfully synthesized. XRD and FT-IR results showed that the incorporation of fillers did not change PVDF's crystal structure and polymer framework. The surface morphology is significantly improved with the appearance of a porous structure and a uniformly dispersed phase. PL spectrum and band gap analysis showed that the SiO_2/g-C_3N_4/PVDF sample can inhibit e^-/h^+ recombination, and the band gap is suitable for visible light absorption. Photocatalytic testing showed that the SiO_2/g-C_3N_4/PVDF sample had the highest RhB degradation efficiency (81.35%), confirming its potential application in organic pollution treatment under visible light.

Acknowledgments

REFERENCES

(1) K. Sun, Q-Y. Lv, X-L. Chen, L-B Qu and B. Recent advances in visible-light-mediated organic transformations in water. *Green Chemistry,* **2021**, *23* (1), 232-248.

(2) H. Lin, J. Wu, F. Zhou, X. Zhao, P. Lu, G. Sun, Y. Song, Y. Li, X. Liu, H. Dai. Graphitic carbon nitride-based photocatalysts in the applications of environmental catalysis. *Journal of Environmental Sciences,* **2023**, *124*, 570-590.

(3) P. B. B. Long, V. C. Nguyen, H. A. Le Pham, Q. T. H. Ta, H. P. Dang. Effect of the Dimethylformamide/Isopropanol Solvent Ratio on the Structure, Optical Properties, and Photodegradation Performance of RhB Using Bi-MOF. *Bulletin of Chemical Reaction Engineering & Catalysis,* **2025**, *20* (1), 166-176.

(4) T. K. A. Nguyen, T. T. Pham, H. Nguyen-Phu, EW. Shin. The effect of graphitic carbon nitride precursors on the photocatalytic dye degradation of water-dispersible graphitic carbon nitride photocatalysts. *Appl. Surf. Sci.* **2021**, *537*, 148027-148038.

(5) Yu. Yutang, H. H. Coupled adsorption and photocatalysis of g-C_3N_4 based composites: Material synthesis, mechanism, and environmental applications. *Chemical Engineering Journal,* **2023**, *453*, 139755.

(6) Q. Hao, X. Niu, C. Nie, S. Hao, W. Zou, J. Ge, D. Chen, W. Yao. Highly Efficient g-C_3N_4/SiO_2 Heterojunction: The role of SiO_2 for the Enhanced Visible Light Photocatalytic Activity. *Phys. Chem. Chem. Phys,* **2016**, *18* (1-25).

(7) X. Wang, S. Wang, W. Hu, J. Cai, L. Zhang, L. Dong, L. Zhao, Y. He. Synthesis and photocatalytic activity of SiO_2/g-C_3N_4 composite photocatalyst. *Materials Letters,* **2014**, *115*, 53-56.

(8) Q. T. H. Ta, G. Namgung, J. S. Noh. Facile synthesis of porous metal-doped ZnO/g-C_3N_4 composites for highly efficient photocatalysts. *Journal of Photochemistry and Photobiology A: Chemistry,* **2019**, *368*, 110-119.

(9) T. Li, L. Zhao, Y. He, J. Cai, M. Luo, J. Lin. Synthesis of g-C_3N_4/$SmVO_4$ composite photocatalyst with improved visible light photocatalytic activities in RhB degradation. *Applied Catalysis B: Environmental,* **2013**, *129*, 255-263.

(10) Y. He, J. Cai, T. Li, Y. Wu, Y. Yi, M. Luo, L. Zhao. Synthesis, characterization, and activity evaluation of $DyVO_4$/g-C_3N_4 composites under visible-light irradiation. *Industrial &*

engineering chemistry research, **2012**, *51* (45), 14729-14737.

(11) S. C. Yan, S. B. Lv, Z. S. Li, Z. G. Zou. Organic–inorganic composite photocatalyst of gC_3N_4 and TaON with improved visible light photocatalytic activities. *Dalton Transactions,* **2010**, *39* (6), 1488-1491.

(12) G. Liu, P. Niu, C. Sun, S. C. Smith, Z. Chen, G. Q. Lu, H. M. Cheng. Unique electronic structure induced high photoreactivity of sulfur-doped graphitic C_3N_4. *Journal of the American Chemical Society,* **2010**, *132* (33), 11642-11648.

(13) X. Chen, J. Zhang, X. Fu, M. Antonietti, X. Wang. Fe-g-C_3N_4-catalyzed oxidation of benzene to phenol using hydrogen peroxide and visible light. *Journal of the American Chemical Society,* **2009**, *131* (33), 11658-11659.

(14) C. Yao, A. Yuan, H. Zhang, B. Li, J. Liu, F. Xi, X. Dong. Facile surface modification of textiles with photocatalytic carbon nitride nanosheets and the excellent performance for self-cleaning and degradation of gaseous formaldehyde. *Journal of Colloid and Interface Science,* **2019**, *533*, 144-153.

(15) J. Zhao, J. Wang, L. Fan, E. Pakdel, S. Huang, X. Wang. Immobilization of titanium dioxide on PAN fiber as a recyclable photocatalyst via co-dispersion solvent dip coating. *Textile Research Journal,* **2017**, *87* (5), 570-581.

(16) L. Peng, W. Chen, B. Su, A. Yu, X. Jiang. $CsxWO_3$ nanosheet-coated cotton fabric with multiple functions: UV/NIR shielding and full-spectrum-responsive self-cleaning. *Applied Surface Science,* **2019**, *475*, 325-333.

(17) C. Shi, J. Zhu, X. Shen, F. Chen, F. Ning, H. Zhang, YZ. Long, X. Ning, J. Zhao. Flexible inorganic membranes used as a high thermal safety separator for the lithium-ion battery. *RSC advances,* **2018**, *8* (8), 4072-4077.

(18) I. Kolesnyk, J. Kujawa, H. Bubela, V. Konovalova, A. Burban, A. Cyganiuk, W. Kujawski. Photocatalytic properties of PVDF membranes modified with g-C_3N_4 in the process of Rhodamines decomposition. *Separation and Purification Technology,* **2020**, *250*, 117231.

(19) K. Prakash, PS. Kumar, P. Latha, K. Saravanakumar, S. Karuthapandian. Design and fabrication of a novel metal-free SiO_2/gC_3N_4 nanocomposite: a robust photocatalyst for the degradation of organic contaminants. *Journal of Inorganic and Organometallic Polymers and Materials,* **2018**, *28*, 268-278.

(20) Y. Shen, X. Guo, X. Bo, Y. Wang, X. Guo, M. Xie, X. Guo. Effect of template-induced surface species on electronic structure and photocatalytic activity of g-C_3N_4. *Applied Surface Science,* **2017**, *396*, 933-938.

(21) Z. Mo, X. She, Y. Li, L. Liu, L. Huang, Z. Chen, Q. Zhang. Synthesis of g-C_3N_4 at different temperatures for superior visible/UV photocatalytic performance and photoelectrochemical sensing of MB solution. *RSC advances*, **2015,** *5*(123), 101552-101562.

(22) B. Zhu, P. Xia, Y. Li, W. Ho, J. Yu, Fabrication and photocatalytic activity enhanced mechanism of direct Z-scheme g-C_3N_4/Ag_2WO_4 photocatalyst. *Applied Surface Science,* **2017**, *391*, 175-183.

(23) Z. Vilamova, P. Czernek, J. Zagora, L. Svoboda, J. Bednar, Z. Simonova, D. Placha, R. Dvorsky. Fibrous PVDF membranes modified by anchored g-C_3N_4@ GO composite with enhanced photocatalytic activity. *Applied Surface Science,* **2024**, *677*, 161055.

(24) Y. J. Kim, C. H. Ahn, M. B. Lee, M. S. Choi. Characteristics of electrospun PVDF/SiO_2 composite nanofiber membranes as polymer electrolyte. *Materials Chemistry and Physics,* **2011**, *127* (1-2), 137-142.